Supplementary information: On-chip dual quantum walk comb in the mid-infrared

Miguel Montesinos-Ballester[*1], Lucius Miller[1], Emilio Gini[2], Mattias Beck[1] and Jérôme Faist[1]
[1]*Institute for Quantum Electronics, ETH Zurich, 8093 Zürich, Switzerland*
[2]*FIRST Center for Micro- and Nanosciences, ETH Zurich, 8093 Zürich, Switzerland*
[*]e-mail: mmontesinos@ethz.ch

1. Coupling simulations

To estimate the coupling between both resonators, optical simulations are performed with the cut-view profile obtained by scanning electron microscope (SEM) images in an equivalent resonator pair fabricated next to the one used in this work (Supplementary Figure 1(a)). The finite difference eigenmode (FDE) solver of Lumerical (Ansys) is used to obtain the guided modes of the coupling resonator section. Then, the power coupling coefficient is calculated as $|\kappa|^2 = \sin^2\left(\frac{\pi \cdot L \cdot \Delta n_{eff}}{\lambda}\right)$, where L is the 1 mm coupling length and Δn_{eff} is the effective refractive index difference between the symmetric and anti-symmetric modes of TM polarization, as the geometry of both optical waveguides is similar. As observed in Supplementary Figure 2(b), power coupling between resonators below 2×10^{-5} is expected in the wavelength range under consideration. Since the coupling between resonators is smaller than the detuning between each of the comb line pairs, both cavities are effectively decoupled.

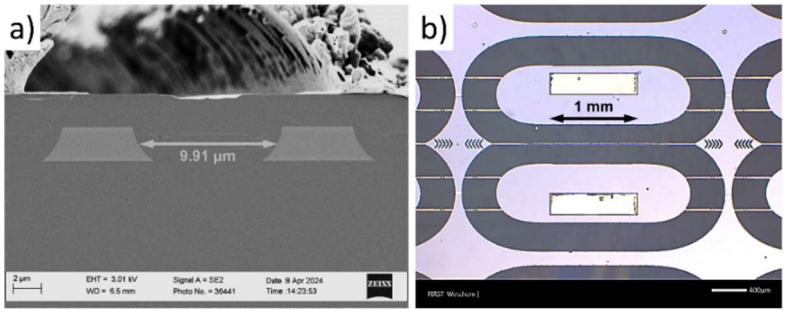

Supplementary Figure 1 | Fabricated sample. (a) Cut-view SEM image of the two resonators in the adjacent straight section, measured in an equivalent device fabricated next to one used in this work. **(b)** Top-view image of the two resonators in the sample before cleaving.

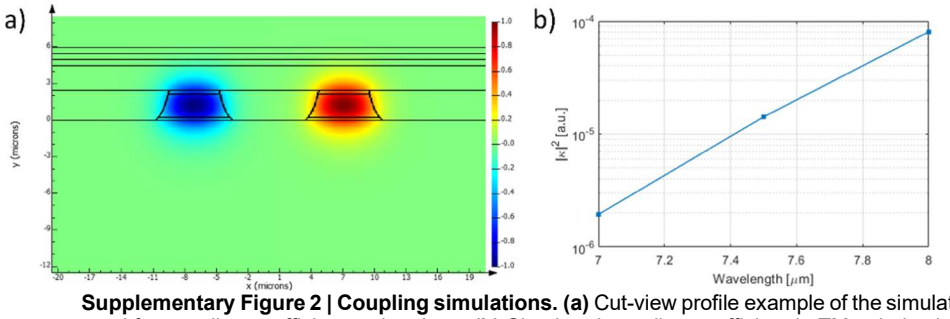

Supplementary Figure 2 | Coupling simulations. (a) Cut-view profile example of the simulations used for coupling coefficient estimations. **(b)** Simulated coupling coefficient in TM polarization as a function of the wavelength for 1 mm length coupling section.

2. RF crosstalk between resonators

In preliminary experiments, long metallic wires were bonded directly from the SMA connector to the bottom resonator, and as far as possible from the front resonator (Supplementary Figure 3(a)). Then, the DC was swept from 970 to 1300 mA while the emission spectra recorded in a FTIR spectrometer. Although DC is injected only through the back resonator (furthest to the collecting lens), the top InP cladding is heavily Si-doped and will conduct the DC with a measured resistance of 0.2 Ω between resonators in non-lasing operation. At the same time, an RF amplifier was used and a fixed 19 dBm tone at 13.346 GHz injected into the sample, through the back resonator. The resonant frequencies of both resonator are swept by the DC tuning, eventually matching the injected and fixed RF tone. As observed in Supplementary Figure 3(b), near 38 cm^{-1} wavenumber optical broadening is achieved in the bottom resonator, while only nearly 9 cm^{-1} wavenumber is achieved in the front resonator. Since the RF fades rapidly through the sample, the front resonator experiences minimal optical broadening, proving a minimal RF crosstalk.

It should also be noted that due to the relative detuning of the resonant frequencies between both resonators, the resonant cavities are additionally detuned to respect the RF tone injected in the opposite resonator. Hence, even lower RF influence is assumed in the dual-comb experiments reported in this work. For instance, Supplementary Figure 8(b) shows that, despite the strong RF injection, optical broadening is only observed in one resonator.

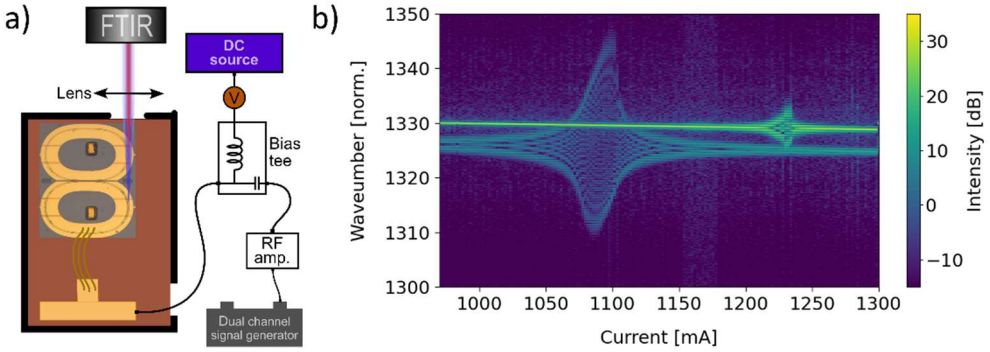

Supplementary Figure 3 | RF crosstalk. (a) Setup schematic used for preliminary experiments where only the bottom resonator was wire bonded to an SMA connector through long wires. An FTIR spectrometer was used to obtain the emitted spectra. **(b)** Spectral emission as a function of the DC bias while a 19 dBm tone at 13.346 GHz is injected.

3. Spectral map as a function of DC bias

The operating DC is characterized by obtaining the spectral map emitted from the right side of the device with a commercial FTIR spectrometer as a function of DC bias that is injected through the font resonator. As observed in Supplementary Figure 4, the back laser (furthest to the collecting lens) has a slightly higher threshold current, which is attributed small deviations in the fabrication process via wet-etching patterning step or thermal dissipation differences across the sample. Since the light emitted from the back laser has to propagate through the sample 1.1 mm further than the front resonator, the emitted optical intensity is slightly attenuated. Therefore, it is possible to clearly distinguish the light emitted from each laser: higher intensity from the from resonator and weaker intensity from the back resonator.

In the initial lasing range, bi-directional operation is produced and multimode formation is observed. When increasing the DC, symmetry breaking is produced and only one direction is sustained, thus single line emission is observed for the highest

injected currents. For instance, a pair of single emission lines separated by 0.86 cm-1 wavenumber (~5 nm wavelength) are observed at 1100 mA of DC, indicated as vertical dashed line.

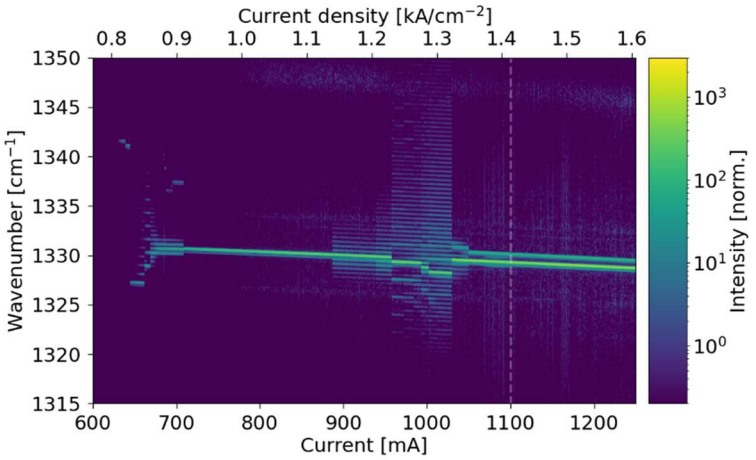

Supplementary Figure 4 | Spectral map as a function of DC. Spectral emission from the right side of the sample as a function of the DC injected and measured in a FTIR spectrometer. The current density is calculated considering two resonators of 6.7 mm length and 5.8 µm width.

4. Device output beam

Since the output light is collected from scattering of sharp waveguide bends, it is important to verify the output beam shape. To that end, a bolometric mid-IR beam profiler (WinCamD-IR-BB, DataRay) is placed after the collecting lens of 4 mm focal length. As observed in Supplementary Figure 5(a), a collimated Gaussian-like far-field is obtained on the beam profiler. A top-view image of the mounted resonator pair inside the nitrogen-purged laser box is also shown in Supplementary Figure 5(b), to observe the practical distance and position of the collecting lens. These images have been taken from an equivalent device, but similar beam spots have been observed in the device used for this work. This is also a clear indication of repeatability of this work.

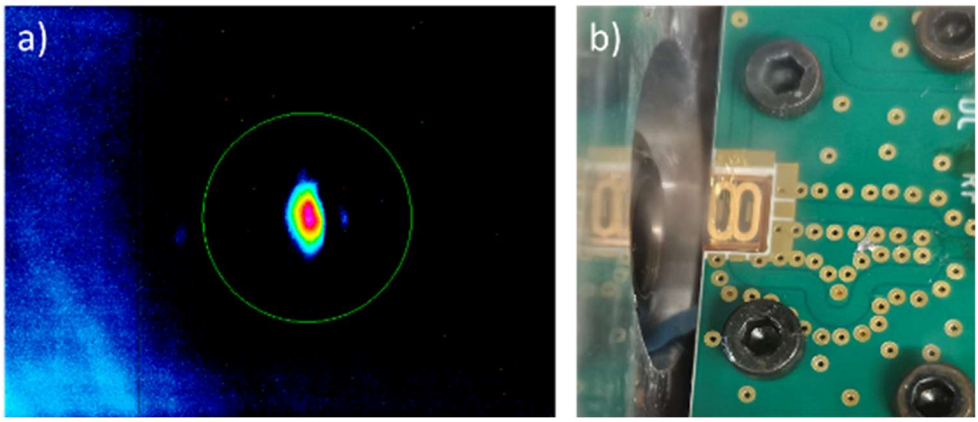

Supplementary Figure 5 | Beam shape and top view image. (a) Output beam captured in a mid-IR beam profiler in a similar device as the one used for the experiments. **(b)** Top view image of the device and position of the collecting lens (in the left-side).

It must be noted that due to a 1.1 mm distance between the resonators centers, and therefore their light emission points, the focal distance for each resonator differs.

Therefore, it is not possible to optimize the output coupling of both resonators at the same time, and the focal length position of the lens may slightly balance the output power between them. Nevertheless, relatively high coupling efficiency is achieved, and optical powers higher than 300 μW (0.3 mA) were measured in a pyroelectric optical power detector. As the dual-comb measurements here reported show, this output power is enough to provide a good SNR of the RF-comb via an electrically-cooled MCT detector (non-cryogenic), meaning a sufficient extraction efficiency and beam overlap from both resonators.

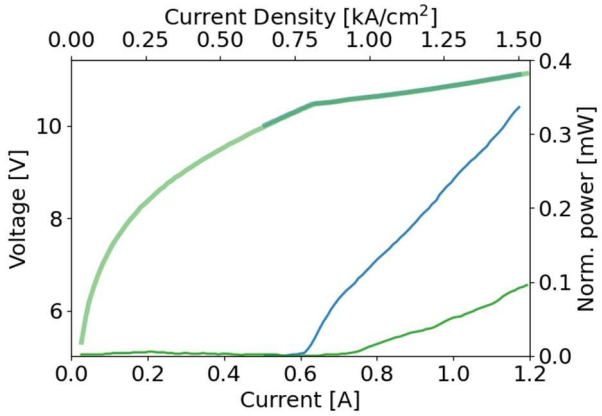

Supplementary Figure 6 | LIV measurements. LIV measurements performed with a pyroelectric optical power meter. Blue and green colors represent the two possible directions of the light propagation after the symmetry breaking is produced.

As observed in Supplementary Figure 6, spontaneous symmetry breaking selects one of the two degenerate propagation directions of the light inside the resonator, with maxima (blue) or minima (green) of scattered light from the side of the sample from which it is being measured. To select a specific correct lasing direction (clockwise or concouter-clockwise), ramping down to currents below threshold and ramp up again must be performed, or the position of the collecting lens moved from right to left side (or vice-versa).

5. Quantum walk comb bandwidth

The power delivered by the two-channel RF source (SynthHD PRO, Windfreak) is experimentally evaluated by measuring the output power of one channel after a bias tee in a spectrum analyzer equipment. This value means the maximal power that can be injected into each device connector of the PCB, individually accessing both racetrack resonators. As observed in Supplementary Figure 7, the RF source is limited to a maximal power of 12.2 dBm at 13.35 GHz. It has been observed that if only one channel is activated (instead two), the maximal RF power that can be delivered near 13.35 GHz is increased by 1.2 dB (up to a maximum of 13.4 dBm). It must be noted that additional RF losses are expected due to the PCB circuit, connectors and wire bonds. In this regard, the use of an additional RF amplifier is required to increase the comb bandwidth.

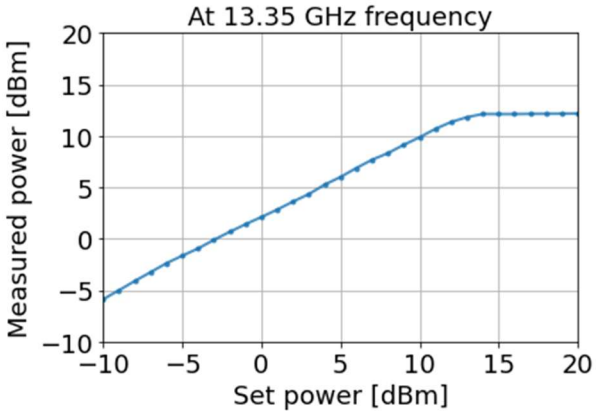

Supplementary Figure 7 | Power delivered by the RF source. Measured power in one RF channel as a function of the set power at 13.35 GHz frequency operation and with both output channels activated.

Supplementary Figure 8 shows the possibility to increase the comb bandwidth with the use of RF amplifiers. First, two single line emission is obtained when 1200 DC and no RF is injected (Supplementary Figure 8(a)). Then, if only one RF tone with an estimated power of 27 dBm is injected into the back resonator, one QWC and one single-line emission with modulated sidebands are obtained (Supplementary Figure 8(b)). Then, if a second tone of 30 dBm is additionally added to the front resonator, two QWC are obtained (Supplementary Figure 8(c)). Although the two RF tones are initially intended to have the same power, so produce similar QWC bandwidth, the non-optimized PCB design and the T-junction used to detect the electrical beat note introduce an estimated 3 dB losses, causing an asymmetric RF injection efficiency. To be able to obtain the emission spectrum from both resonators, a commercial FTIR spectrometer with a high numerical aperture collecting lens are employed.

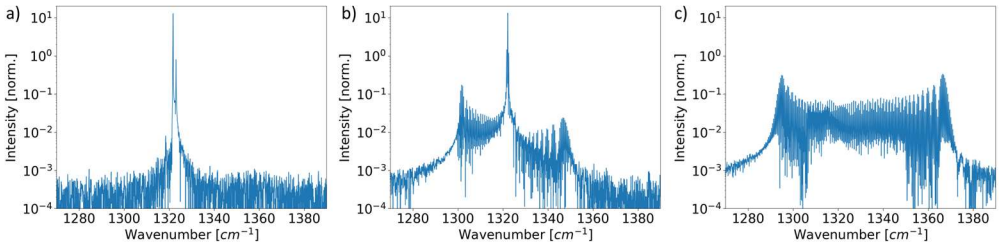

Supplementary Figure 8 | Comb expansion via RF amplification. Optical spectra obtained in a FTIR spectrometer from the right side of the sample when 1200 mA of DC is injected and **(a)** no RF is injected, **(b)** an RF with an estimated power of 27 dBm is injected into the back resonator, and **(c)** an RF with an estimated power of 30 dBm is additionally injected into the front resonator (same as Figure 3 of the manuscript).

6. Numerical noise correction

A 20 ms interferogram at 1200 mA DC and dual RF injection at the resonant frequency with 29 dBm of estimated power provide a relatively good SNR. For instance, Supplementary Figure 9 shows the interferogram detected in the oscilloscope and a clear spectral signal is obtained by simply performing the Fourier-transform of the entire interferogram in forward configuration with a Blackman-Harris window. The background signal is also shown, which has been obtained by collecting a similar interferogram, but blocking the mid-IR beam heading to the fast MCT detector. The

maximum spectral bandwidth is limited to 1.25 GHz by the Nyquist-Shannon theorem, considering the 2.5 GS/s sampling rate of the oscilloscope.

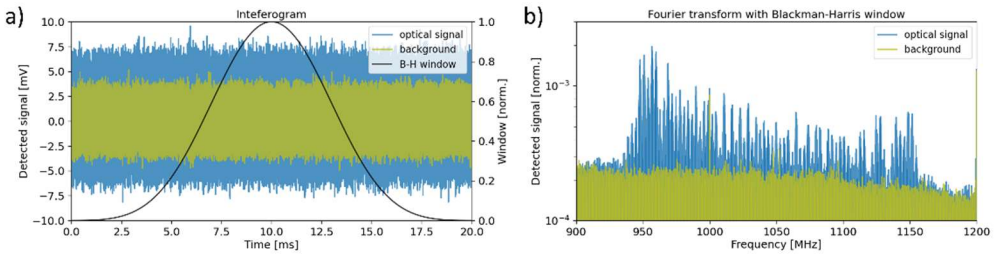

Supplementary Figure 9 | Detected dual-comb signal. (a) Interferogram recorded in the oscilloscope with 1200 mA DC and 29 dBm estimated RF power injected in each resonator. The background signal is also recorded by blocking the beam and the window used in the Fourier-transform is shown. **(b)** Direct Fourier-transform of the interferogram applying a Blackman-Harris window.

As demonstrated in Fig. 4 of the article, the f_{rep} noise can be neglected due to the fact that both QWCs are RF-driven. Nevertheless, the SNR can still be improved by reducing the f_{ceo} noise with the following data analysis. First, the strongest peak is identified near 956 MHz and a bandpass filter is applied. Then, a short-time Fourier-transform (STFT) with 3.2 µs time window is performed with a Blackman-Harris window and 50% step overlap. Next, the peak position of the tone is tracked along the 20 ms trace and its position value is obtained, as shown in Supplementary Figure 10(b).

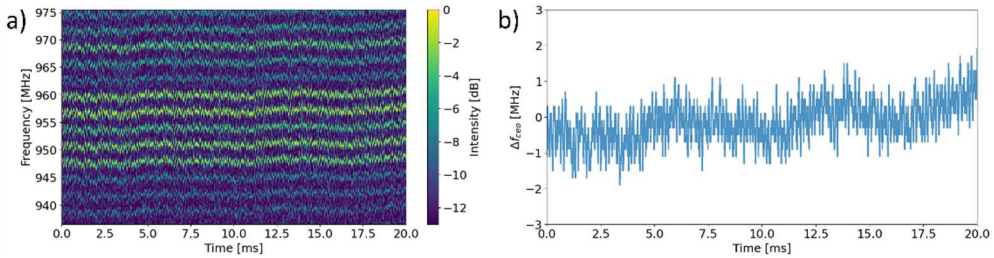

Supplementary Figure 10 | STFT and frequency noise. (a) Zoom-in near the maximum peak value of the STFT of the detected signal. Blackman-Harris moving window with 50% overlap and 3.2 µs width has been used. **(b)** Frequency shift of the highest peak from its average value at each temporal step of the 20 ms trace.

Once the tone offset is obtained with respect to its average value, and since the negligible f_{rep} noise ensures equidistant comb lines, the STFT can be corrected numerically by shifting the RF comb at each time step with the opposite sign. The corrected STFT is shown Supplementary Figure 11.

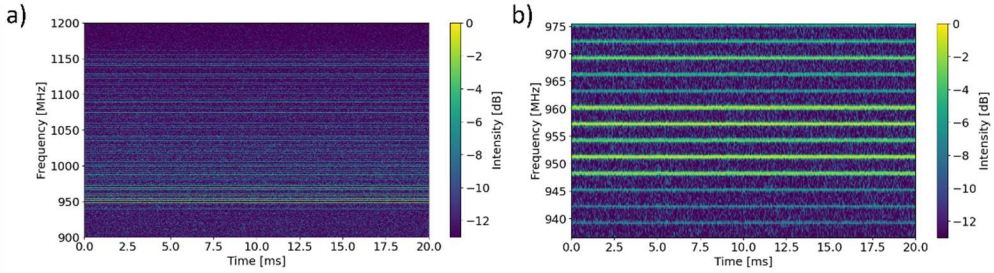

Supplementary Figure 11 | STFT with numerical noise correction. **(a)** Numerically corrected STFT of the optical dual-comb signal. **(b)** Zoom-in near the highest intensity peak.

Next, the numerically corrected SFTF can be averaged across the entire 20 ms trace. As observed in Supplementary Figure 12 and compared with Supplementary Figure 9, an improved SNR is achieved. This procedure is similarly performed to the multi-heterodyne electrical signals directly recorded from the sample and the signals obtained with molecular absorption. It must be noted that for the background signal, the noise correction is not implemented, but only STFT and time averaging. To record the electrical background, the DC current of the laser is detuned from 1200 mA to 1000 mA, so that no dual-comb electrical signal is present. Finally, the respective backgrounds are extracted to the optical and electrical signals.

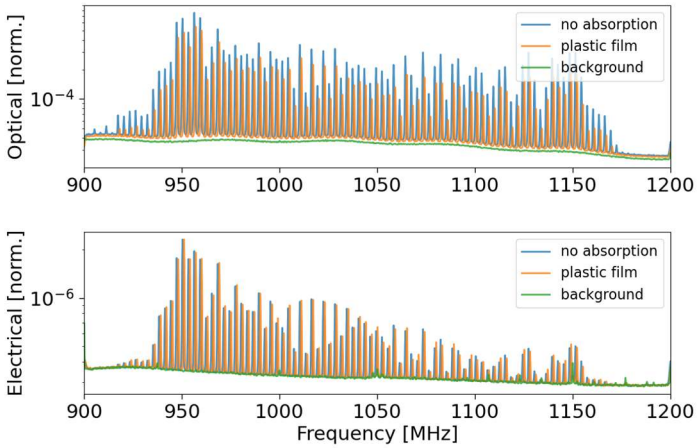

Supplementary Figure 12 | Time averaged corrected signal. Averaged signal of the corrected STFT of the optical, electrical and background signal obtained.

7. Allan deviation

The Allan deviation [37, 38] of the 20 ms time trace without any molecular absorption at 1200 mA DC and dual RF injection at the resonant frequency with 29 dBm of estimated power that is captured in the MCT photodetector can be computed to show that, at least at the time scales of our measurement, the amplitude and frequency of a down-converted from the optical to the RF domain comb tooth is primarily affected by noise which can be averaged out. This may prove advantageous in a resource-constrained real-time measurement setup, where stabilization may only be done computationally rather than through locking to a reference cell.

To that end, we recompute the STFT of the 20 ms time trace using a 3.2 μs long Blackman-Harris window without overlap. By tracing the frequency and amplitude of five strong peaks located near 950 MHz, and computing the overlapped Allan variance [39], we obtain Supplementary Figure 13. The variance data has been cut off above 10 ms averaging time, since at those trace lengths most of the averages significantly overlap. As can be seen in Supplementary Figure 13(a), the frequency begins to drift on very small timescales due to the free-running nature of the combs. This means that signal post-processing may be required to obtain the amplitude profile of the RF signal. However, as in Supplementary Figure 13(b), the variance of the tracked amplitudes keep overall decreasing for averaging times beyond a millisecond.

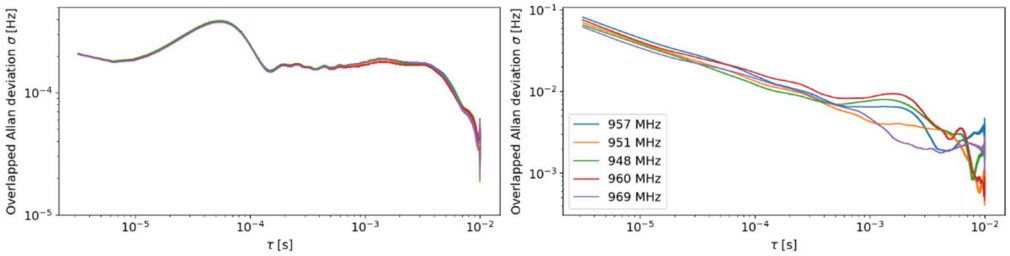

Supplementary Figure 13 | Allan deviation. Double-logarithmic plot of the Allan deviation of the frequency **(a)** and amplitude **(b)** of the tracked peaks. Error bars represent $\sqrt{N}$-errors for the average over the overlapped intervals.

8. Dual-comb spectroscopy proof-of-concept of a methane gas cell

The data processing to retrieve the transmittance from the dual-comb signal at 1200 mA DC and dual RF injection at the resonant frequency with 29 dBm of estimated power is as follows. First, optical (from the MCT detector) and electrical (from the sample) interferograms are recorded simultaneously during 20 ms. This measurement is performed with and without the plastic film between the dual-comb source and MCT detector. Next, the two measurements (w/o plastic film) are split into 10 segments of 2 ms duration. Then, as previously described in Supplementary Section 6, the f_{ceo} noise is numerically corrected and the background is subtracted from the optical and electrical signals of each 2 ms trace. Once the different peaks are identified in each time trace, the transmittance is obtained as $T = \frac{S_p \,/\, S_{p,e}}{S_o \,/\, S_{o,e}}$, where S_o and $S_{o,e}$ are the optical and electrical peak values without molecular absorption normalized to the background, respectively, and S_p and $S_{p,e}$ the normalized optical and electrical peak values with a plastic film, respectively. Finally, the average and standard deviation of the transmittance over the 10 traces of 2 ms are obtained and shown in Fig. 7b of the manuscript.

The frequency axis is also translated from the RF (MHz units) to the optical (wavenumber units) domain, assuming that each datapoint (peak position) is separated by the repetition frequency of 13.35 GHz (0.45 cm^{-1} wavenumber). In order to properly locate the dual-comb spectrum, a flip mirror is used when performing the measurements to obtain the optical spectrum in a commercial FTIR spectrometer. It must be noted that, since the optical beam is optimized to maximize the signal in the MCT fast photodetector, only one of the two QWC is observed. Nevertheless, it is sufficient to identify the spectral position of the dual-comb signal.

The spectral transmission of the plastic film is also obtained with a commercial FTIR spectrometer using its internal broadband light source. A reference trace without molecular absorption and background noise by blocking the optical beam are also recorded and shown in Supplementary Figure 14. Then, the transmittance is obtained as the ratio between molecular absorption medium and no absorption reference trace, shown in Fig. 7b of the manuscript in grey color. Additionally, a 14 cm-length gas cell filled with 1% of methane and 99% of Nitrogen at 1.05 mBar was characterized with the commercial FTIR spectrometer, and later used for a spectroscopy proof-of-concept in Supplementary Section 9.

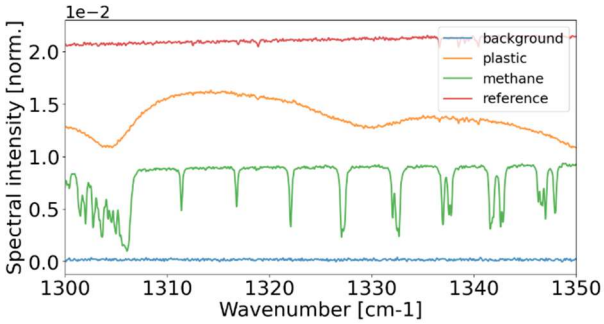

Supplementary Figure 14 | Reference transmission spectrum. Transmission of the 14 cm length gas cell with 1% of methane, a plastic film, background and reference transmission without absorption medium. A commercial FTIR spectrometer has been used, placing the absorption medium in the sample compartment.

9. Dual-comb spectroscopy of a methane gas cell

A proof-of-concept spectroscopy of a plastic film and a methane gas cell has also been performed using the entire 20 ms interferogram trace as follows.

First, optical (from the MCT detector) and electrical (from the sample) interferograms at 1200 mA DC and dual RF injection at the resonant frequency with 29 dBm of estimated power are simultaneously recorded, with and without molecular absorption. In this example, a 14 cm length gas cell filled with 1% of methane and 99% of N_2 was introduced in the optical path, but an equivalent procedure has been performed for the undefined plastic film. Next, the f_{ceo} noise is numerically corrected and the background subtracted, as previously described in Supplementary Section 6. Results are shown in Supplementary Figure 15.

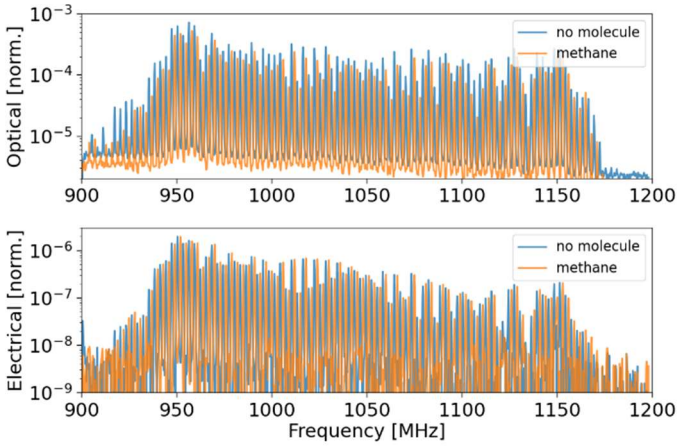

Supplementary Figure 15 | Normalized signal with and without methane absorption. Numerically corrected optical and electrical signals, with and without a 14 cm gas cell filled with 1% of methane in the optical path.

Since the interferograms with and without molecular absorption medium (i.e., methane gas or plastic film) are recorded in different times, a slight variation in the f_{ceo} difference between the two combs causes a minor frequency shift of the dual-comb signal. Also, the f_{ceo} noise correction previously described does not consider the frequency shift between interferogram traces at different times, but only within a given interferogram. Therefore, instead of simply identify the peaks as in Supplementary Section 8 and Fig. 7b of the manuscript, the frequency offset is now first corrected by detecting the highest peak of the comb lines and numerically compensate its frequency

axis difference. As shown in Supplementary Figure 16, an excellent overlap is achieved in the electrical dual-comb signal, while a decrease in the optical signal is observed due to the presence of the methane gas cell. Then, the peaks of the optical dual-comb signal without methane absorption are identified, selecting only the peaks that are 10 dB above the noise floor (dashed line in Supplementary Figure 16). For each frequency position of those peaks, the corresponding value of the optical signal with molecular absorption and electrical dual-comb signals are obtained. It must be noted that a two datapoints with methane absorption where no electrical dual-comb peak was present are removed from the obtained transmission spectra, as they do not represent reliable information.

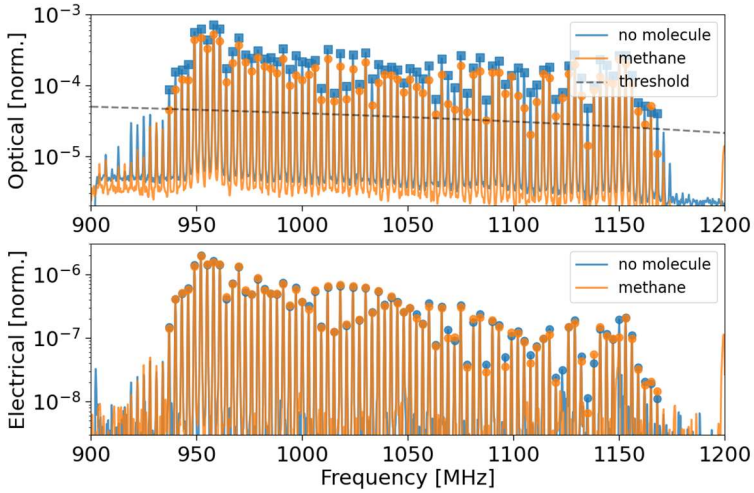

Supplementary Figure 16 | Dual-comb signal overlap and peak identification. Detected and processed dual-comb signals with and without a methane gas cell, where the frequency axis difference between them has been numerically suppressed. The position of the peaks of the optical signal without molecular absorption is obtained (squared markers) with a threshold above the noise floor of 10 dB. At each frequency position of the peaks, the corresponding optical signal with methane absorption and electrical signals are obtained and shown as round markers.

Finally, as in Supplementary Section 8, the transmittance is obtained as the ratio between optical and electrical peak values normalized to the background noise, with and without methane absorption, respectively, and the frequency axis translated to wavenumber. This procedure is performed for the methane gas cell and plastic film. A spectral transmission reference is also obtained with a commercial FTIR spectrometer and its internal broadband light source, shown in Supplementary Figure 14. It must be noted that, as the methane gas cell has a length of 14 cm and 1-inch angled windows, the optical beam of the commercial FTIR spectrometer may be partly blocked, reducing the intensity of the reference transmission spectrum obtained for methane. Therefore, to better compare the absorption features, the normalized methane transmission obtained with the commercial FTIR spectrometer is increased by a factor of 2.5 dB. The results are observed in Supplementary Figure 17, where the transmittance closely follows the broad absorptions of the plastic film and sharp methane absorption features are observed. Since the dual-comb source is effectively sampling the molecular absorptions, the reference transmittance is also sampled at the repetition frequency of 13.35 GHz (0.45 cm^{-1} wavenumber) to better compare the results.

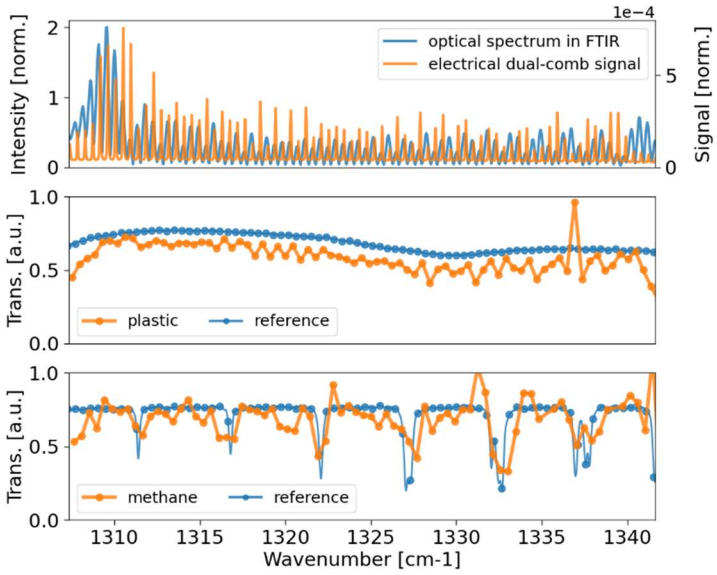

Supplementary Figure 17 | Spectroscopy proof-of-concept. Top panel: optical spectrum obtained with a commercial FTIR spectrometer (left y-axis) and dual-comb signal (right y-axis) with the frequency axis converted to wavenumber. Middle panel: normalized transmission spectra for a plastic film placed in the optical path obtained with the dual-comb source and a commercial FTIR spectrometer. Bottom panel: similar transmission spectra, using a 14 cm-length gas cell with 1% methane. A 2.5 dB factor has been applied to the methane reference signal (in blue) to better compare the results.